Minerals Engineering 216 (2024) 108854

Contents lists available at ScienceDirect

Minerals Engineering

journal homepage: www.elsevier.com/locate/mineng

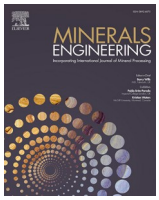

Pre-reduction of Nchwaning manganese ore in CO/CO_2, H_2/H_2O, and H_2 atmospheres

M.S. ERNST [a], M. TANGSTAD [b], S.P. DU PREEZ [a,*]

[a] Hydrogen South Africa (HySA) Infrastructure, Faculty of Engineering, North-West University (NWU), Potchefstroom Campus, Private Bag X6001, Potchefstroom, 2520, South Africa
[b] Department of Material Science and Engineering, Norwegian University of Science and Technology (NTNU), Alfred Getz Vei 2, Trondheim, 7034, Norway

ARTICLE INFO

Keywords:
Manganese
Hydrogen
Ferromanganese
Pre-reduction

ABSTRACT

Hydrogen (H_2), a relatively underexplored reductant in ferromanganese (FeMn) production, offers an attractive avenue for mitigating gaseous carbon (C) emissions. The reduction behaviour of South African Nchwaning manganese (Mn) ore using gaseous CO/CO_2, H_2/H_2O, and H_2 atmospheres was investigated experimentally in the temperature variation of 700, 800, and 900 °C. The effect of different gas compositions and temperatures was studied using a vertical thermogravimetric (TG) tube furnace. During pre-reduction, two parallel reactions occurred, namely the reduction of higher Mn- and iron (Fe) -oxides, and the decomposition of carbonates. After each test, decrepitation, chemical composition, phase transformation, and porosity were characterised. Using the rate of mass loss, a kinetic model was obtained to predict kinetic constants. The oxidation state of the higher Mn- and Fe-oxides was lowered during CO/CO_2 and H_2/H_2O pre-reduction. Only during pure H_2 pre-reduction was Fe^{2+} reduced to its metallic state, Fe^0. The majority of carbonates decomposed in the presence of the CO/CO_2 atmosphere at 900 °C, whereas in the presence of H_2 in the reducing atmosphere carbonates decomposed at a higher rate and lower temperatures. Additionally, the extent and rate of mass loss were expedited by increasing the temperature, employing H_2-containing atmospheres, and lowering the oxygen partial pressure (pO_2) of the H_2-containing atmospheres. No significant trends were observed in ore decrepitation and porosity across various atmospheres and temperatures, except for decrepitation in the water vapour-containing atmosphere. The utilisation of a pure H_2 atmosphere has a significant ability for pre-reducing Mn ores with carbonate content by expediting carbonate decomposition and promoting Fe-oxide metallisation, thereby enhancing the efficiency of ore treatment in metallurgical applications.

1. Introduction

Manganese ferroalloy production accounts for 90 % of the world's Mn production and is mainly used in the steel industry (Olsen et al., 2007; Pochart et al., 2007). As a result, the trends in steel production directly impact the demand for Mn ferroalloy production, which typically accounts for approximately 1 % of overall steel production (Cheraghi et al., 2020). The addition of Mn to steel offers several advantages due to its low cost and abundance. Mn decreases brittleness, enhances hardenability, desulphurise, and deoxidise, and improves the strength and abrasion resistance of steel (Davies et al., 2023; Olsen et al., 2007). Thus, Mn is a vital metal in steel production, due to its industrial advantage. There are three main groups of Mn ferroalloys produced, which are defined based on the final composition and specifications. These groups are silicomanganese (SiMn), high-carbon FeMn (HC-FeMn), and refined FeMn. The latter is divided into medium- and low-carbon FeMn (MC-FeMn and LC-FeMn) (Cheraghi et al., 2020). The Fe constituent of these alloys originates from the Fe-oxides present in the raw ore.

The production of FeMn occurs in two distinct types of furnaces, categorised by the manganese-to-iron mass ratio (Mn/Fe). Blast furnaces (BFs) are typically used when the ore has a Mn/Fe of < 6.2, whereas submerged arc furnaces (SAFs) are used for ores with a Mn/Fe of > 6.2 (Eissa et al., 2012). In 2014, global BF-based Mn ferroalloy production was a mere 0.5 Mmt, whereas in 2021 it was reported as only 0.2 Mmt (Corathers, 2017, 2023). It can be seen that BF-based production is systematically being phased out of operation (Vogl et al., 2021).

On the other hand, SAF-based production has the advantage of the

* Corresponding author.
E-mail address: faan.dupreez@nwu.ac.za (S.P. DU PREEZ).

https://doi.org/10.1016/j.mineng.2024.108854
Received 4 April 2024; Received in revised form 5 July 2024; Accepted 16 July 2024
Available online 25 July 2024

flexibility of their product and production capacities (Bergman & Kjellberg, 2001). A SAF has two zones, namely, the pre-reduction zone (upper part) and the smelting zone (lower part) (Larssen & Tangstad, 2022; Ngoy et al., 2020). Raw materials are fed from above and systematically descend from the pre-reduction zone to the smelting zone. Solid C sources, such as coke, or anthracite are used as the reductant, which is found in the smelting zone. The pre-reduction zone is defined as the zone where the raw materials are in the solid state, thus the temperature is less than 1200 °C (Larssen & Tangstad, 2022). Here, the higher Mn- and Fe-oxides are pre-reduced to lower Mn- and Fe-oxides by carbon monoxide (CO), formed in the smelting zone. The smelting zone is the hottest part of the furnace, with temperatures ranging from 1300 – 2000 °C (Eric, 2014). These temperatures facilitate the reduction of the lower Mn- and Fe-oxides with C to form CO, which permeates upwards to the pre-reduction zone, as well as the melting of the pre-reduced ores and fluxes to form the molten alloy and slag phase.

The reactions in the pre-reduction zone are the reduction of the higher Mn-oxides (MnO_2, Mn_2O_3 and Mn_3O_4) by CO (Reactions 1 – 3) and the reduction of the higher Fe-oxides (Fe_2O_3 and Fe_3O_4) by CO (Reactions 4 and 5). Gaseous carbon dioxide (CO_2) is formed as the by-product.

$$2MnO_2(s) + CO(g) = Mn_2O_3(s) + CO_2(g),\ \Delta H^\circ_{298K}=\text{-}202\ kJ/mol \quad (R1)$$

$$3Mn_2O_3(s) + CO(g) = 2Mn_3O_4(s) + CO_2(g),\ \Delta H^\circ_{298K}=\text{-}177\ kJ/mol \quad (R2)$$

$$Mn_3O_4(s) + CO(g) = 3MnO(s) + CO_2(g),\ \Delta H^\circ_{298K}=\text{-}53\ kJ/mol \quad (R3)$$

$$Fe_2O_3(s) + CO(g) = 2Fe_3O_4(s) + CO_2(g),\ \Delta H^\circ_{298K}=\text{-}40\ kJ/mol \quad (R4)$$

$$Fe_3O_4(s) + CO(g) = 3FeO(s) + CO_2(g),\ \Delta H^\circ_{298K}=31\ kJ/mol \quad (R5)$$

The MnO and FeO are reduced by solid C to Mn and Fe metal in the smelting zone (Reactions 6 and 7). The Boudouard reaction is also present, as the CO_2 will react with the solid C, at temperatures higher than 800 °C (Reaction 8) (Olsen et al., 2007).

$$MnO(s) + C(s) = Mn(s) + CO(g),\ \Delta H^\circ_{298K}=275\ kJ/mol \quad (R6)$$

$$FeO(s) + C(s) = Fe(s) + CO(g),\ \Delta H^\circ_{298K}=157\ kJ/mol \quad (R7)$$

$$C(s) + CO_2(g) = 2CO(g),\ \Delta H^\circ_{298K}=172\ kJ/mol \quad (R8)$$

The solid-state pre-reduction of higher Mn-oxides is kinetically controlled, and not thermodynamically (Davies et al., 2023). Consequently, factors that affect the rate of pre-reduction include the ore porosity, charge material particle size, furnace heating rate, and the reducing atmosphere (Chen et al., 2020; Ngoy et al., 2020; Schanche & Tangstad, 2021). These operating conditions and material properties affect the specific electric consumption, which ranges from 2400 to 3400 kWh/mt FeMn produced (Olsen et al., 2007). The substantial energy demand is partly due to the endothermic nature of the Boudouard reaction (Reaction 8). This reaction consumes a significant amount of energy, leading to energy losses within the furnace. (Cheng et al., 1999; Kalenga et al., 2013).

Alternative routes have been explored in recent years to mitigate gaseous carbon release to the atmosphere during traditional ferroalloy production (Davies, Paktunc, et al., 2022a; Davies, Tangstad, et al., 2022b; Du Preez et al., 2023; Tangstad et al., 2023). For FeMn producers, environmental pressure to curb gaseous carbon release, as well as increasing carbon taxes being levied by governments is the main driving force. Recent studies have been done on pre-reducing Mn ore with H_2, considering that the only by-product is water vapour (Davies et al., 2023; Larssen & Tangstad, 2022; Ngoy et al., 2020; Schanche & Tangstad, 2021). This approach also circumvents the occurrence of the highly endothermic and carbon consuming Boudouard reaction.

The H_2-based reactions will be similar to CO-based reduction: the higher Mn-oxides (MnO_2, Mn_2O_3 and Mn_3O_4) are reduced to lower Mn-oxides by H_2 (Reactions (9) to (11)).

$$2MnO_2(s) + H_2(g) = Mn_2O_3(s) + H_2O(g),\ \Delta H^\circ_{298K}=\text{-}157\ kJ/mol \quad (R9)$$

$$3Mn_2O_3(s) + H_2(g) = 2Mn_3O_4(s) + H_2O(g),\ \Delta H^\circ_{298K}=\text{-}140\ kJ/mol \quad (R10)$$

$$Mn_3O_4(s) + H_2(g) = 3MnO(s) + H_2O(g),\ \Delta H^\circ_{298K}=\text{-}10\ kJ/mol \quad (R11)$$

The complete reduction of MnO to Mn metal by gaseous H_2 is thermodynamically unfavourable, as it would require infeasible operation temperatures. Therefore, C would still be implemented to metallise MnO. Nevertheless, considering that Fe-oxides are major constituencies of Mn ores, their metallisation by H_2 is possible under normal operation conditions (Reactions (12) and (13)) (Davies et al., 2023).

$$Fe_2O_3(s) + H_2(g) = 2FeO(s) + H_2O(g),\ \Delta H^\circ_{298K}=47\ kJ/mol \quad (R12)$$

$$FeO(s) + H_2(g) = Fe(s) + H_2O(g),\ \Delta H^\circ_{298K}=25\ kJ/mol \quad (R13)$$

When simplifying the SAF-based production (Reactions 1–7), it results in 3 mol of gaseous carbon by-products. In contrast, the alternative route (Reactions 6, 9–13) results in 1 mol of gaseous carbon by-products. Thus, theoretically, the alternative route results in a 67 % decrease in gaseous carbon production.

Ngoy et al. (2020) investigated the non-isothermal reduction of Nchwaning and Comilog Mn ores over a temperature range of 25 – 1000 °C, in four reducing atmospheres (50 %CO/50 %CO_2, 70 %CO/30 %CO_2, 41 %CO/41 %CO_2/18 %H_2, and 41 %CO/18 %CO_2/41 %H_2) with two distinct pO_2 profiles. It was found that for similar pO_2 profiles, the reduction rate increased by 20 – 30 % when H_2 was included in the reducing atmosphere. Furthermore, the reduction rate increased when the pO_2 profile decreased, regardless of whether H_2 was present in the reducing atmosphere (Ngoy et al., 2020).

Schanche & Tangstad (2021) investigated the isothermal reduction of Nchwaning Mn ore at three temperatures (600, 700, and 800 °C) in four reducing atmospheres (30 %CO/70 %CO_2, 70 %CO/30 %CO_2, 16 % CO/68 %CO_2/16 %H_2, and 37 %CO/26 %CO_2/37 %H_2) with two distinct pO_2 profiles. Similar to the previous results, it was found that an increase in temperature and a decrease in the pO_2 profile improved the extent and rate of reduction. Furthermore, the inclusion of H_2 increased the reduction rate by a factor of 1.3 and 2.6 for low and high pO_2 profiles, respectively. It is believed that this was due to improved diffusion characteristics of H_2 (Schanche & Tangstad, 2021).

Larssen & Tangstad (2022) investigated the non-isothermal reduction of Nchwaning and Comilog Mn ores over a temperature range of 25 – 800 °C, in five reducing atmospheres (50 %CO/50 %CO_2, 44 %CO/44 %CO_2/13 %H_2, 56 %CO/31 %CO_2/13 %H_2O, 70 %CO/17 %CO_2/13 % H_2, and 80 %CO/20 %–CO_2) with two distinct pO_2 profiles. The influence of moisture on the reduction kinetics was investigated by including H_2O, and the subsequence water–gas shift reaction (WGSR). Similar to previous results, it is found that the highest extent of reduction is obtained at a lower pO_2 profile H_2-containing atmosphere. With regards to the WGSR, equilibrium is only reached at higher temperatures (Larssen & Tangstad, 2022).

Davies et al. (2023) investigated the isothermal reduction of United Manganese of Kalahari (UMK) Mn ore at three temperatures (700, 800, and 900 °C) in three reducing atmospheres (70 %CO/30 %CO_2, 70 %H_2/ 30 %H_2O, and 100 %H_2) with two distinct pO_2 profiles. Similar to previous results, it is found that the inclusion of H_2 increases the reduction rate, but also the decomposition rate of the carbonates. Both rates are further accelerated by increasing the temperature. More so, the 100 %H_2 atmosphere facilitated Fe-metallisation from Fe-oxides present in the ore (Davies et al., 2023). As UMK ore is considered a carbonate-rich ore, it is unsurprising that most mass loss during reduction is due to carbonate decomposition. In a carbonate-poor ore, such as Nchwaning ore, carbonate decomposition will be less prominent, which could affect the mass loss rate. Take note that Nchwaning ore is yet to be subjected to isothermal reduction at temperatures ranging from 700 – 900 °C in the presence of 70 %H_2/30 %H_2O and 100 %H_2 reducing

atmospheres.

This study investigates the effect of temperature and reducing atmospheres on the mass loss rate of Nchwaning Mn ore. This ore originates from South Africa (SA), where 75 % of global Mn resources are found (Corathers, 2020). Nchwaning ore is considered carbonate-poor, with 0.82 – 4.8 mass% carbonates, and semi-oxidised ore, with an oxygen-to-manganese mass ratio (O/Mn) of approximately 1.47 (Larssen et al., 2021; Ngoy et al., 2018; Visser et al., 2013). The mass loss is continuously measured during isothermal experimentation in a TG tube furnace in the presence of 70 %CO/30 %CO_2, 70 %H_2/30 %H_2O, and 100 %H_2 atmospheres. The CO/CO_2 atmosphere serves as a reference to previous work and compares to the H_2/H_2O atmosphere in terms of the pO_2 profile in the 700 – 900 °C temperature range. The comparability in the pO_2 profile is an indication of similar thermodynamic driving forces in pre-reduction and carbonate decomposition reactions. The pure H_2 atmosphere has a lower pO_2 profile in the same temperature range, thus, Fe-metallisation is expected in this atmosphere.

2. Materials And Methods

2.1. Experimental

Nchwaning Mn ore (N′Chwaning Mine, SA) was used in this study. The general composition of Nchwaning ore includes braunite (3(Mn,Fe)$_2O_3$•$MnSiO_3$), braunite II (7(Mn,Fe)$_2O_3$•$CaSiO_3$), bixbyite ((Mn,Fe)$_2O_3$), hematite (Fe_2O_3), hausmannite (Mn_3O_4), calcite ($CaCO_3$) magnesite ($MgCO_3$) and dolomite ($CaMg(CO_3)_2$) where the former three minerals are major Mn-containing phases. The utilised gasses are Ar (99.999 %), CO (99.97 %), CO_2 (99.9992 %) and H_2 (99.9 %), purchased from Linde. The H_2O vapour is produced in an evaporator by pressurising distilled water with a helium bladder system.

A sample of 10 kg was randomly selected from a batch of Nchwaning ore and was then crushed with a Retsch BB300 jaw crusher for 1.5 h. After sieving there was 6.7 kg of the 9.5 – 16 mm size fraction. This is the required size fraction for this series of experiments. This fraction was dried at 105 °C for 5 h to remove any potential surface moisture. Thereafter, the dried ore sample was divided into individual batches of 150 g with a riffle-splitting technique. The dried and divided ore is from now on referred to as the raw ore.

The mass loss during reduction of the raw ore was measured with an Entech VTF 80/15 TG vertical resistance tube furnace. Before and after each experiment, the mass of each batch was recorded using an Ohaus Pioneer PA4202 scale, to confirm the net mass loss from the TG data. A raw ore batch of 150 g was placed in a gas-tight and temperature-resistant stainless-steel (253 MA) double-wall crucible. The crucible has a length of 45 cm and an inside diameter of 4.8 cm. After the charge is added, a K-type thermocouple is placed in an alumina tube and positioned in the middle of the charge. This thermocouple measures the temperature that the charge experiences during the experiment. Next, the crucible is sealed and suspended from a Mettler Toledo PR2003DR balance to record the mass fluctuations during operation. Flexible gas inlet and outlet pipes are connected to the screw top of the crucible to enable the crucible to move freely. The gas flow rate during every stage of the experiment is kept constant at 4 nL/min. The hollow double-wall of the crucible, where the gas is pre-heated and homogenised, is given in Fig. 1.

The furnace position can be vertically altered, which enables the uninterrupted functioning of the suspended crucible. The furnace hot zone has a height of 68 cm and a length and width of 36 cm. A 65 °C temperature difference between the charge and furnace temperature was observed during prior testing. Thus, for the charge in the crucible to be at the correct experimental temperature (i.e., 700, 800, and 900 °C), the furnace is preheated to the respective temperature setpoints (i.e., 635, 735, and 835 °C) at a rate of 41 °C/min. The furnace heating is controlled by a Eurotherm PID controller and measured with a calibrated S-type thermocouple. All reported temperatures were measured

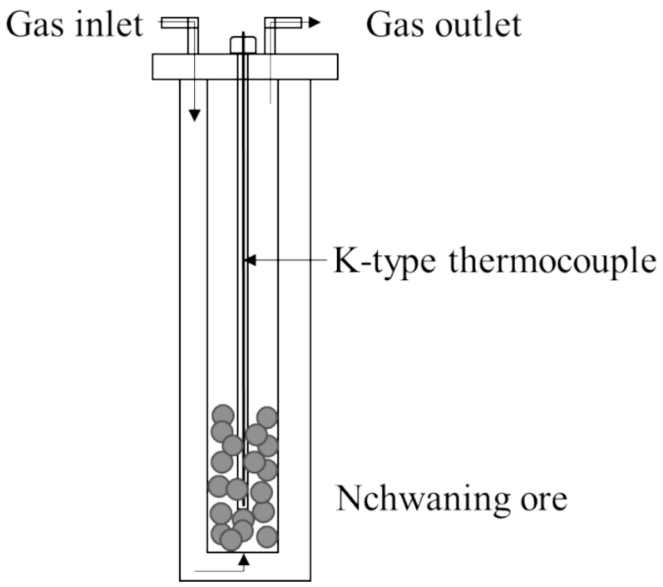

Fig. 1. The gas flow, raw Nchwaning ore, and the K-type thermocouple inside the crucible.

using the K-type thermocouple, as this is the true temperature experienced by the charge. The furnace was preheated in the raised position which enables the simultaneous preheating of the suspended crucible and charge material. While preheating took place, Ar was used to prevent premature pre-reduction.

When the furnace reached the temperature setpoint, the charge temperature inside the crucible was given 15 min to reach the experimental temperature. Hereafter, Ar was changed to the respective reducing gas atmosphere. Each gas line is controlled by a Bronkhorst F-201C mass flow controller. The furnace was kept in the raised position until the charge mass stabilised, meaning the reactions between the ore and the gas atmosphere had concluded. The reduction time, depending on the temperature, and gas atmosphere, ranged from 90 to 300 min.

After the reduction phase had concluded, the furnace was lowered, and the reducing gas atmosphere was changed back to Ar. After the crucible and charge had cooled down to ambient temperature, it was removed from the suspenders. The reacted charge is recovered for further characterisation. The set-up for this furnace is depicted in Fig. 2.

Some degree of thermal carbonate decomposition took place during the preheating phase. To account for mass loss from carbonate decomposition during the heating phase, three experiments were conducted. The crucible is charged with the raw ore and heated in Ar to 700, 800, and 900 °C, respectively, at the same rate, i.e., 41 °C/min, as the reduction experiments. After the 15 min to reach the temperature setpoint, the experiment ended as described in the paragraph above. As a form of validation and accuracy measurement, inert quarts were tested beforehand in the same way as the raw ore in the same atmospheres, i.e., 70 %CO/30 %CO_2, 70 %H_2/30 %H_2O, and 100 %H_2 at 900 °C. The results showed mass loss of < 0.1 %.

For each of the three investigated reducing atmospheres, each temperature was evaluated in duplicate. A summary of the experiments is given in Table 1. Note that all reported values are the average of duplicates. Each recovered pre-reduced sample is handled separately, to link differences in chemical compositions to the unique mass loss profiles.

Particle size distribution (PSD) analysis served two goals namely, to separate the sample into two homogeneous parts and to measure decrepitation. Size partitioning was conducted by manually sieving samples through a stack of sieves consisting of sizes 9.5, 6.7, 4.75, 3.15, 1.6, and 0.5 mm. The mass in each size interval is weighed, whereafter each size interval is divided through riffle-splitting. Each half of each

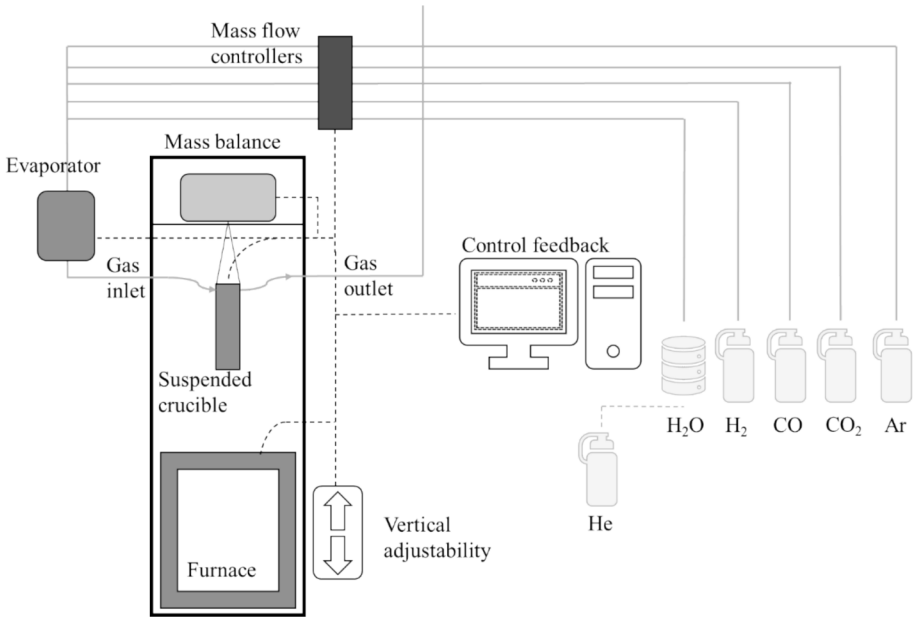

Fig. 2. The set-up of the Entech VTF 80/15 TG vertical resistance tube furnace.

Table 1
A summary of the conducted experiments.

Gas atmosphere	Temperature [°C]		
	700	800	900
100 %Ar	Ar-700A	Ar-800A	Ar-900A
70 %CO/30 %CO_2	CO/CO_2-700A	CO/CO_2-800A	CO/CO_2-900A
	CO/CO_2-700B	CO/CO_2-800B	CO/CO_2-900B
70 %H_2/30 %H_2O	H_2/H_2O-700A	H_2/H_2O-800A	H_2/H_2O-900A
	H_2/H_2O-700B	H_2/H_2O-800B	H_2/H_2O-900B
100 %H_2	H_2-700A	H_2-800A	H_2-900A
	H_2-700B	H_2-800B	H_2-900B

size interval is remixed, resulting in two evenly divided samples from the original pre-reduced sample. One half is used for chemical analysis and the other half is used for phase transformation analysis and porosity measurements, as depicted in Fig. 3.

The chemical composition of the raw and pre-reduced ores was examined by performing x-ray fluorescence (XRF) analyses with a Bruker S4 Pioneer x-ray fluorescence spectrometer using the fused bead technique. Permanganometric titration (ASTM 465–11:2017) was employed to measure the amount of O_2 bonded to Mn, which is expressed as MnO_2. The C content was analysed with a LECO (Combustion-IR) instrument, and the CO_2 content was determined by assuming that all C in the ore is in the form of CO_2. The loss on ignition (LOI) was thermogravimetrically measured to a stable mass at 950 °C in air.

The raw and pre-reduced samples are prepared for x-ray diffraction (XRD) analysis by grinding the samples with a Retch vibratory disc mill RS 200 at 900 rpm for 90 s. This grinding set consists of tungsten carbide grinding rings and a plate. XRD analysis was performed on the pulverised raw and pre-reduced ores by using a Bruker D8 A25 DaVinci x-ray diffractometer with CuKα radiation and a LynxEyeTM SuperSpeed detector. The results were obtained in a total of 7200 s at a scanning angle of 2θ and a range of 10 – 90° with 0.013° step sizes. The DIFFRAC.EVA V6.1 software together with the PDF-4 + database was used to index the phases present in the samples. The amorphous content was not measured as it is assumed that the majority of the ore is crystalline.

Porosity measurements were performed on three randomly selected particles from the raw and pre-reduced samples. The porosity was determined by the ratio between the absolute and apparent density. The

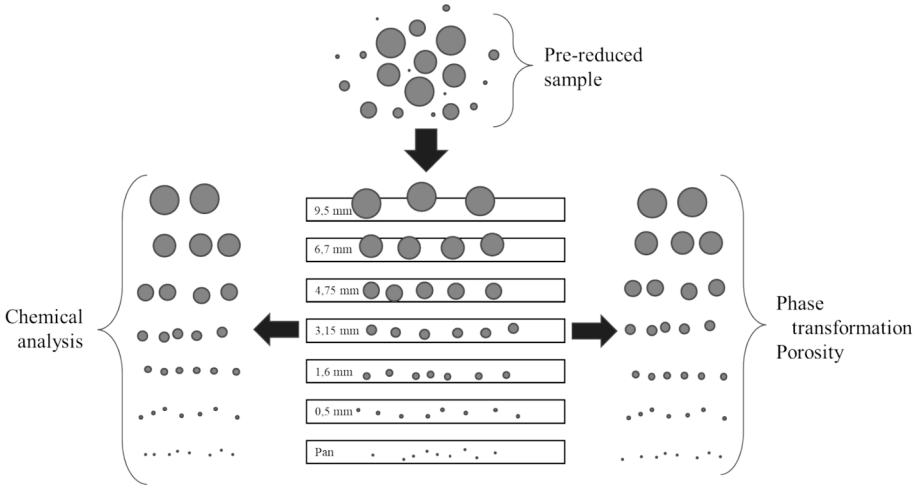

Fig. 3. Size partitioning of the pre-reduced sample.

absolute density was measured by an Accupyc 1330 He pycnometer, while the apparent density was determined by a GeoPyc 1360 pycnometer.

2.2. Calculations

The mass loss during reduction is continuously measured at a time series of 5 s. The corresponding O/Mn as a function of time (O/Mn(t)) is calculated using Equation 1 with the mass loss percentage at time t (ml.%(t)), the applicable theoretical mass loss percentage (theo.ml.%), and the initial O/Mn (O/Mn$_{(i)}$). The O/Mn$_{(i)}$ is calculated from the chemical analysis of the raw ore, where the Mn was determined through XRF, and the MnO_2 was measured by the above-mentioned titrimetric method. The O/Mn$_{(i)}$ value is calculated using Equations 2 and 3 when assuming that all the Mn absent in MnO_2 is present in MnO. Note that n(A) denotes the amount of moles of A.

$$O/Mn(t) = O/Mn_{(i)} - (O/Mn_{(i)} - 1)(ml.\%(t))/(theo.ml.\%) \quad (E1)$$

$$n(MnO) = n(Mn) - n(MnO_2) \quad (E2)$$

$$O/Mn_{(i)} = [2n(MnO_2) + n(MnO)]/n(Mn) \quad (E3)$$

The theo.ml.% is calculated from the chemical analysis of the raw ore, specifically the LOI, CO_2, O/Mn and Fe content of the ore. Three assumptions are made namely: i) all the Fe is initially in the form of Fe_2O_3 and reduced to FeO or Fe, ii) Mn reduces from O/Mn$_{(i)}$ to MnO and iii) all the C present in the raw ore represents carbonates that will decompose to CO_2. As mentioned, the LOI is measured at 950 °C, and it is assumed that at this temperature all present carbonates have decomposed, all present volatiles evaporated, and the most stable higher Mn-oxide is Mn_3O_4. Hence, the LOI contains water vapour, carbonates and Mn_3O_4. The theoretical mass loss for Nchwaning ore is calculated with Equations 4 – 6. Note that M(A) denotes the molecular mass of A and that μ(A)$_{(i)}$ denotes the mass percentage of A in the raw material.

$$Fetheo.ml.\% = (FeO_{1.5} - FeO_1)M(O)\mu(Fe)_{(i)}/M(Fe) \quad (E4)$$

$$Mntheo.ml.\% = (O/Mn_{(i)} - 1)M(O)\mu(Mn)_{(i)}/M(Mn) \quad (E5)$$

$$H_2Otheo.ml.\% = LOI_{950} - \mu(CO_2)_{(i)} - (O/Mn_{(i)} - 1.33)M(O)\mu(Mn)_{(i)}/M(Mn) \quad (E6)$$

The extent of pre-reduction is presented as α and is calculated from the measured mass as a function of time t in mass percentage, (μ(t)), and the maximum mass loss percentage (ml.%$_{(max)}$) using Equation 7.

$$\alpha = \mu(t)/ml.\%_{(max)} \quad (E7)$$

When α = 0, no pre-reduction or decomposition has taken place, whereas α = 1 suggests complete pre-reduction of higher Mn- and Fe-oxides to MnO, FeO, or Fe, and complete carbonate decomposition. The rate, r, of pre-reduction and carbonate decomposition, is derived by differentiating α with respect to t, as shown in Equation 8. This is numerically calculated by determining the slope between each value of α as a function of time with the central difference formula.

$$r_j = \partial\alpha/\partial t \approx (\alpha_{j+1} - \alpha_{j-1})/(t_{j+1} - t_{j-1}) \quad (E8)$$

Thermodynamic calculations are done by using HSC Chemistry 10 and FactSage and include the phase stability diagrams of the Mn- and Fe-oxides together with the reducing atmospheres and of the carbonates. The reported enthalpy values were calculated with HSC Chemistry 10.

3. Results And Discussion

3.1. Chemical composition

The chemical composition results from the raw and pre-reduced ore in the reducing atmospheres in the 700 – 900 °C temperature range is summarised in Table 2.

The raw Mn ore contains around 41 mass% Mn and is therefore considered medium-grade Mn ore (Acharya et al., 2004). The O/Mn$_{(i)}$, LOI$_{950}$, Mn/Fe, basicity (B_{CMSA}), and theoretical mass loss are calculated from the raw ore results. The O/Mn$_{(i)}$ is calculated as 1.48, which indicates that the Mn-oxides are predominantly in the Mn_2O_3 form and that the case study ore is a semi-oxidised ore. After reduction, trace amounts of MnO_2 were measured, resulting in an O/Mn of 1.00 according to Equations 2 and 3. This suggests that the atmosphere is reducing enough for the reduction of higher manganese oxides to MnO.

The LOI$_{950}$ of the raw ore is 6.21 mass% and the Mn/Fe of the raw ore was calculated as 2.7. The B_{CMSA} of the raw ore was calculated as 2.2, suggesting that the case study ore has a relatively high basicity. A high basicity results in a low MnO content, 15 – 20 %, after reduction, as well as a high MnO activity for a low MnO content MnO-CaO-SiO_2 slag. This Mn ore will be suitable for the discard slag method, also called the flux method (Tangstad, 2013). The theoretical mass loss of the raw ore was calculated with Equations 4 (Fe), 5 (Mn), and 6 (H_2O), from the chemical composition results, and is given in Table 3.

As mentioned in Section II-B, it is assumed that there will be different extents of Fe reduction in the different reducing atmospheres. This is a necessary differentiation, as the total theoretical mass loss will be used in further calculations. Another differentiation to make is the phases during which carbonate decomposition occurred, namely both the heating and pre-reduction phases. Carbonate decomposition is explained at the hand of the phase stability diagram of the carbonates generally present in Nchwaning Mn ore, which is given as the CO_2 partial pressure (pCO_2) as a function of temperature in Fig. 4.

From Fig. 4 it is seen that magnesite ($MgCO_3$), rhodochrosite ($MnCO_3$), and dolomite ($CaMg(CO_3)_2$) thermally decompose at low temperatures, similar to the temperature during the heating phase. Calcite ($CaCO_3$) only decomposes at much higher temperatures. In the presence of an atmosphere where the pCO_2 = 0.3 bar, such as the 70 % CO/30 %CO_2 atmosphere, these carbonates decompose at 272, 308, 389, and 810 °C, respectively.

To account for the carbonate decomposition during the heating phase, the mass loss was measured as 2.06, 3.34, and 3.04 mass%. for 700, 800, and 900 °C, respectively, in the three Ar heating experiments. The expected mass loss from carbonate decomposition is 4.10 wt% as shown in Table 3. Thus, 50 – 80 % of carbonate decomposition occurs during the heating phase and is completed during the pre-reduction phase. Only 20 – 50 % of the theoretical mass loss from carbonate decomposition is included in the O/Mn(t) calculation. Carbonate decomposition is expected to contribute 6 – 20 % of the mass loss for all the atmospheres and temperatures. The theoretical and measured mass loss for each reducing atmosphere is given in Table 4 and the fraction of carbonate decomposition during pre-reduction is given in Fig. 5.

From Fig. 5 it is evident that in the CO/CO_2 atmosphere, the average carbonate decomposition, presented with dashed lines, correlates directly with temperature. As shown in Fig. 4, at a pCO_2 = 0.3 bar, $MgCO_3$, $MnCO_3$ and $CaMg(CO_3)_2$ is completely decomposed at temperatures ≤ 700 °C, while $CaCO_3$ decomposes only at 810 °C. The increase in the decomposition fraction over the temperature range is primarily due to $CaCO_3$ decomposition.

In contrast to CO/CO_2 pre-reduction, increasing temperature hardly affects carbonate decomposition during pre-reduction in H_2-containing atmospheres, which ranged from 86 % to 96 % over the 700 – 900 °C temperature range. The pCO_2 is low compared to that of the CO/CO_2 atmosphere and consequently, there is a higher driving force for carbonate decomposition (Criado et al., 1982; Valverde et al., 2015; Wang et al., 2007). This high driving force results in rapid decomposition rates, and thus an increase in temperature from 700 to 900 °C has an insignificant effect on the fraction of decomposition.

In general, temperature directly influences the fraction of carbonate decomposition, as displayed during the Ar heating phase and the CO/CO_2 pre-reduction. In this case, the carbonates decompose from only a

Table 2
Chemical composition [mass%] of raw and pre-reduced Nchwaning ore.

Chemical compound	Raw ore	Reducing atmospheres and Temperature [°C]								
		70 %CO/30 %CO_2			70 %H_2/30 %H_2O			100 %H_2		
		700	800	900	700	800	900	700	800	900
C	1.12	1.36	0.52	0.12	0.13	0.06	0.03	0.09	0.05	0.04
CO_2	4.10	5.00	1.90	0.42	0.46	0.20	0.11	0.31	0.19	0.14
Mn	40.80	47.08	55.33	53.22	48.78	54.44	54.51	53.67	56.51	54.57
Fe	15.02	10.26	10.32	9.7	12.54	7.59	9.01	9.85	9.15	9.64
SiO_2	3.63	5.32	2.94	4.33	4.9	5.45	3.71	4.16	3.99	5.95
Al_2O_3	0.24	0.34	0.29	0.56	0.29	0.58	0.4	0.49	0.52	0.69
CaO	7.58	9.73	5.76	8.96	9.65	8.39	8.9	9.32	7.93	9.09
MgO	0.95	2.21	0.66	1.92	1.62	2.1	1.72	1.16	1.37	1.47
P	0.02	0.02	0.02	0.05	0.03	0.03	0.02	0.02	0.03	0.04
S	0.05	0.2	0.18	0.17	0.08	0.05	0.09	0.15	0.22	0.17
TiO_2	<0.03	<0.03	<0.03	<0.03	<0.05	<0.03	<0.03	<0.03	<0.03	<0.08
K_2O	<0.03	<0.03	<0.05	<0.03	<0.03	<0.07	<0.03	<0.05	<0.03	<0.05
BaO	0.09	0.73	0.5	0.29	0.34	0.22	0.54	0.76	0.65	0.27
MnO_2	31.03	<0.05	<0.05	<0.05	<0.05	<0.05	<0.05	<0.05	<0.05	<0.05

Table 3
The theoretical mass loss [mass%] of raw Nchwaning ore as calculated from the chemical composition analysis of the raw ore.

Theoretical mass loss	[mass%]
Pre-reduction of O/$Mn_{(i)}$ to MnO	5.71
Pre-reduction of $FeO_{1.5}$ to FeO	2.15
Pre-reduction of $FeO_{1.5}$ to Fe	6.45
Carbonate decomposition	4.10
H_2O evaporation	0.32

small amount of heat exposure due to an extremely low pCO_2, as in the case of the heating phase. These results are similar to those of Davies et al., (2023).

3.2. Extent and rate of mass loss

The extent, α, and rate, r, of mass loss over *t* for each temperature under different reducing atmospheres are determined using Equations 7 and 8, and the results are given in Figs. 6 and 7. Note that α and r represent the overall mass loss resulting from multiple reactions during the experiments and not a singular species. The O/Mn and α are closely related, and the results for the O/Mn curves are given in Figure 1 in the Supplementary document. With increasing temperature, the O/Mn declines more rapidly from 1.48 to 1.00. The decline is most pronounced in the presence of 100 %H_2, followed by 70 %H_2/30 %H_2O, and finally, 70 %CO/30 %CO_2. This shows the positive effect of increased temperatures, as well as the inclusion of H_2 in the reducing atmosphere, on the declination rate.

Two significant trends emerge regarding the extent and rate of mass loss as shown in Figs. 6 and 7. Firstly, the reducing atmosphere greatly influences the reduction. The maximum mass loss occurs in the 100 %H_2 atmosphere at 700 °C due to prolonged exposure to the reduction atmosphere, serving as the reference for comparison as in Equation 7. In the presence of pure H_2, both the extent (0.95 – 1) and rate (0.08 – 0.11 min^{-1}) are the highest, due to the rapid reaction between oxides and H_2,

Table 4
Theoretical and measured mass loss [mass%] for the reducing atmospheres over the 700 – 900 °C temperature range.

Reducing atmosphere	Theoretical mass loss	Measured mass loss
70 %CO/30 %CO_2	9.0 – 10.2	7.7 – 10.8
70 %H_2/30 %H_2O	9.0 – 10.2	10.5 – 10.8
100 %H_2	13.3 – 14.5	13.0 – 13.8

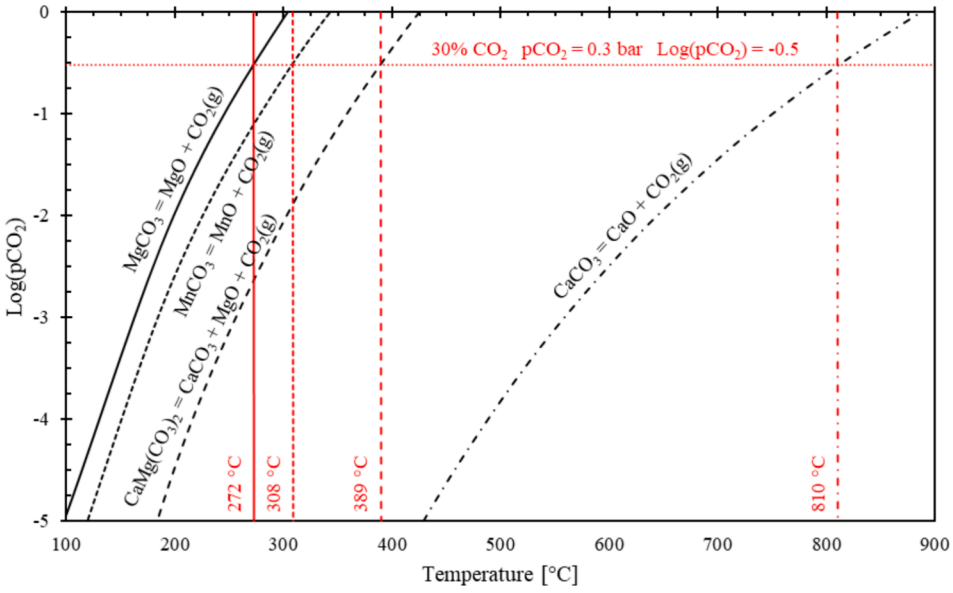

Fig. 4. The phase stability diagram for the present carbonates as pCO_2 as a function of temperature. HSC Chemistry 10 was used to calculate the values (Davies et al., 2023; Schanche & Tangstad, 2021).

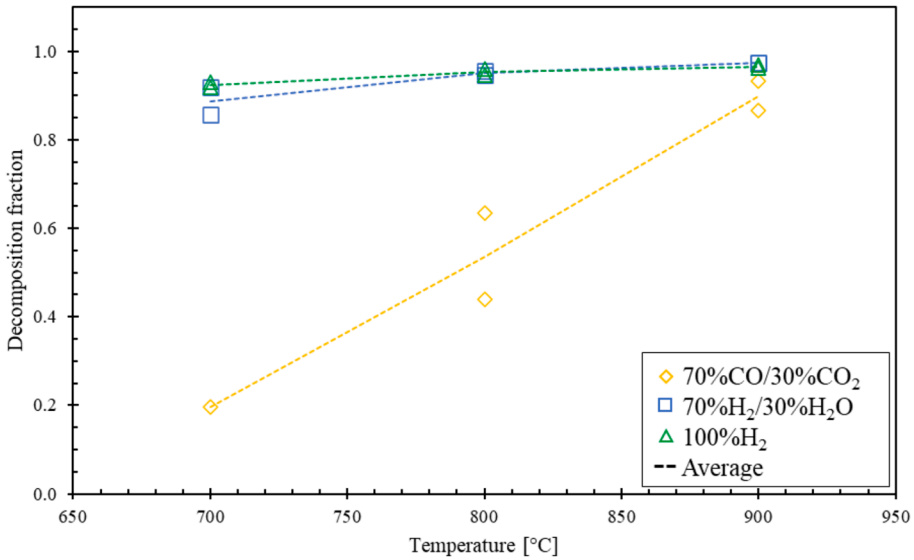

Fig. 5. The carbonate decomposition of the pre-reduced ore under different reducing atmospheres.

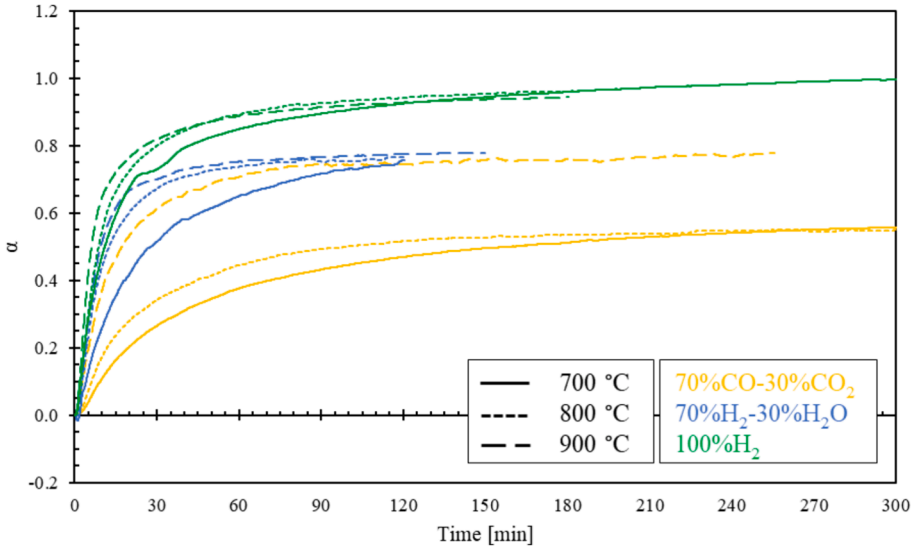

Fig. 6. The extent of mass loss for Nchwaning ore in the different reducing atmospheres at the selected temperatures.

and Fe-metallisation. Davies et al. (2023) also reported Fe-metallisation during 100 %H_2 pre-reduction.

Conversely, in the 70 %H_2/30 %H_2O atmosphere, the extent is 80 % of that in the pure H_2 atmosphere (0.75 – 0.8) due to the higher Fe-oxides being reduced only to FeO. The rate is slightly slower (0.05 – 0.08 min^{-1}) due to the decreased H_2 concentration. In the 70 %CO/30 % CO_2 atmosphere, the extent is lower (0.55 – 0.75) primarily because of a smaller extent of carbonate decomposition, with the slowest rate (0.02 – 0.06 min^{-1}) observed due to sluggish reaction kinetics with CO. Overall, the inclusion of H_2 in reducing atmospheres yields the highest extent and rate of reduction, which is consistent with other studies (Davies et al., 2023; Larssen & Tangstad, 2022; Ngoy et al., 2020; Schanche & Tangstad, 2021).

Secondly, temperature also significantly affects the extent and rate of mass loss. With increasing temperature, the rate increases substantially, by 255 % (CO/CO_2), 56 % (H_2/H_2O), and 49 % (H_2) at their respective peak rate. This is in alignment with other studies conducted at similar temperature ranges (Biørnstad, 2020; Davies et al., 2023; Schanche & Tangstad, 2021). Higher temperatures facilitate more favourable collisions between the H_2 and CO reductants and the oxides and carbonates, leading to faster reaction rates. However, at 700 °C in the 70 %H_2/30 % H_2O atmosphere, partial condensation of water vapour occurs, causing a momentarily negative rate due to increased mass from the liquid phase formation. In practical terms, what is observed here is a dynamic equilibrium between the vapour and liquid phases. Initially, within the first 1 to 3 min, condensation outpaces evaporation, leading to a temporary increase in mass. Subsequently, evaporation accelerates, causing the mass to decrease once more. This cycle of alternating faster condensation and faster evaporation persists until equilibrium between the two phases is attained. Overall, temperature strongly correlates with both the rate of mass loss and equilibrium time.

3.3. *Kinetic modelling.*

Kinetic modelling is done to further analyse the mass loss rate under different reaction conditions. Here, a similar approach as by Schanche & Tangstad (2021) was followed. As previously stated, the rate of the reduction of Mn-oxides is kinetically controlled and not thermodynamically. This means the product ratio is determined by the rate at which the products form rather than the stability of the formed products

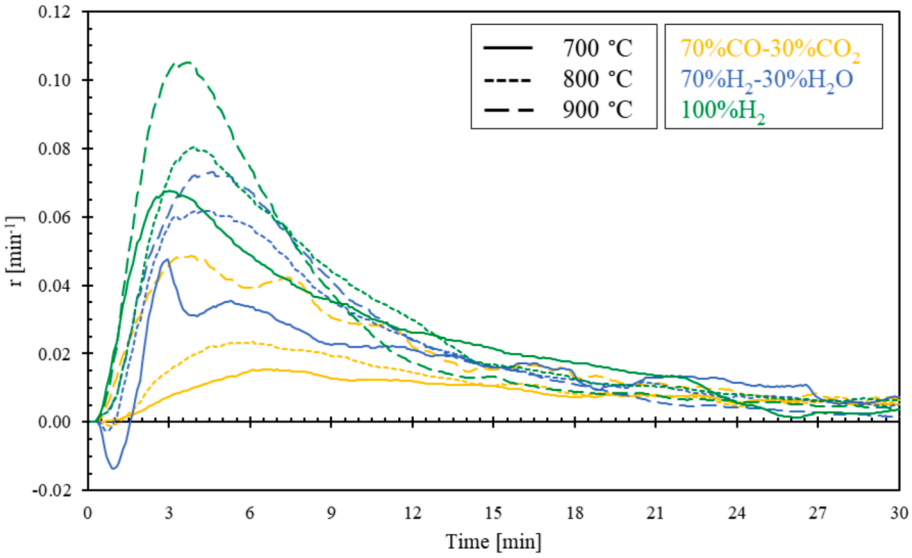

Fig. 7. The rate of mass loss for Nchwaning ore in the different reducing atmospheres at the selected temperatures.

as in thermodynamic controlled reactions. The rate is described in terms of a pre-exponential constant as seen in Equation 9.

$$d\alpha/dt = k_0(1-\alpha)^x \exp(-E_a/RT) \quad \text{(E9)}$$

Here the rate, $d\alpha/dt$, is obtained by the pre-exponential constant, k_0, the extent, α, the reaction order, x, the apparent activation energy, E_a, the universal gas constant, R, and the temperature, T. Here, k_0 represents an overall reaction kinetic constant from the contributions from all the separate pre-reduction reactions during mass loss. The rate increases when k_0 and T are increased and the rate decreases when E_a, x and α are increased. Thus, as the reaction progresses and the extent tends closer to 1, the rate of the reaction slows down. The modelling results are shown in Table 5.

The kinetic model is optimised for the different reducing atmospheres over the investigated temperature range. The fixed model parameters are chosen the same as from a previous study done by Schanche & Tangstad (2021): E_a = 68.1 kJ/mol and x = 2. This method enables the direct comparison of k_0 between the atmospheres and assessing the effect of adding H_2. The model (dashed line) fits the data (solid line) fairly well as seen in Fig. 8 and Table 5.

The CO/CO_2 and H_2/H_2O atmospheres have similar pO_2 profiles, but the inclusion of H_2 in the atmosphere results in an increase in the reduction rate and subsequently the modelled pre-exponential constant by a factor of 2.4 from 49 min^{-1} to 116 min^{-1}. The two H_2-containing atmospheres have a high (70 $\%H_2$/30 $\%H_2O$) and low (100 $\%H_2$) pO_2 profile. Decreasing the pO_2 of an H_2-containing reducing atmosphere increases the reduction rate and thus the pre-exponential constant as well. A decrease by a factor of 5.5 x 10^{-8} for the pO_2 resulted in an increase by a factor of 1.6 on k_0 from 116 min^{-1} to 180 min^{-1}.

In summary, the O/Mn, rate of mass loss, and the calculated pre-exponential constant all behave the same as the varying reducing atmospheres. In atmospheres with the same pO_2 profile, the inclusion of H_2 leads to a faster decline of the O/Mn from 1.48 to 1.00, an increased rate of mass loss, and thus also the pre-exponential constant. Furthermore, for the H_2-containing atmospheres, the decrease of the pO_2 enhances these trends. The rate of mass loss increased with a range of 83 – 300 % and the pre-exponential constant increased by a factor of 3.7 over the three reducing atmospheres.

These findings align with findings by Ngoy et al. (2020), who observed a 20 – 30 % increase in the mass loss rate. Schanche & Tangstad (2021) noted a 1.8-fold increase in the pre-exponential constant when H_2 was introduced to the reducing atmosphere. Additionally, regarding pO_2, studies by Ngoy et al. (2020), Schanche & Tangstad (2021), and Larssen & Tangstad (2022) all concluded that decreasing pO_2 leads to an increased rate of reduction.

Table 5
The modelled pre-exponential constant and correlation coefficient for each reducing atmosphere over the 700 – 900 °C temperature range.

Reducing atmosphere	k_0 [min^{-1}]	R^2
70 $\%CO$/30 $\%CO_2$	49	0.80
70 $\%H_2$/30 $\%H_2O$	116	0.77
100 $\%H_2$	180	0.77

3.4. Mineralogical phase change

As mentioned in Section II-A, the raw ore contains Ca- and Mg-carbonates and Mn- and Fe-oxides in the form of braunite, braunite II, bixbyite, hematite and hausmannite. The former three minerals are the main Mn-containing phases, which suggests that the oxidation state of the Mn before reduction is Mn^{3+} (Mn_2O_3). This was confirmed with the $O/Mn_{(i)}$ of 1.48, as calculated from the chemical analysis, shown in Table 2. This oxidation state, Mn^{3+}, is circled in the stability diagrams for the Mn- and Fe-oxides, given in Fig. 9.

In Fig. 9, the Mn-O (black) and Fe-O (red) stability diagram is shown with the pO_2 as a function of temperature with FactSage (Bale et al., 2016). The databases used were FToxide for slags, glasses, ceramics, and refractories, FTmisc for sulphides, alloys, etc., and FactPS for FACT pure substances. The reducing atmospheres are also shown with their respective pO_2 as a function of temperature with HSC Chemistry 10 (Roine, 2017).. The stability diagram is a tool to understand the trends during the mineralogical phase change of the pre-reduced samples. The results from the XRD analysis of the raw and pre-reduced ore are shown in Fig. 10.

From Fig. 10 it is seen that for the samples pre-reduced in the CO/CO_2 atmosphere, Ca- and Mg-carbonates were detected at 700 and 800 °C, but not at 900 °C. This correlates with the thermodynamic considerations in Fig. 5, suggesting calcite's decomposition at 810 °C in a pCO_2 = 0.3 bar atmosphere. At 700 °C, the peak intensity for the braunite/bixbyite phase decreased, and no hematite and hausmannite were detected, as these higher Mn- and Fe-oxides reduced to MnO and FeO. At 800 °C, no braunite/bixbyite, hematite, and hausmannite was detected. The MnO and FeO peaks have, as a result, a higher peak intensity than at 700 °C. At 900 °C, only MnO and FeO are detected.

For samples pre-reduced in the H_2/H_2O atmosphere, no carbonates

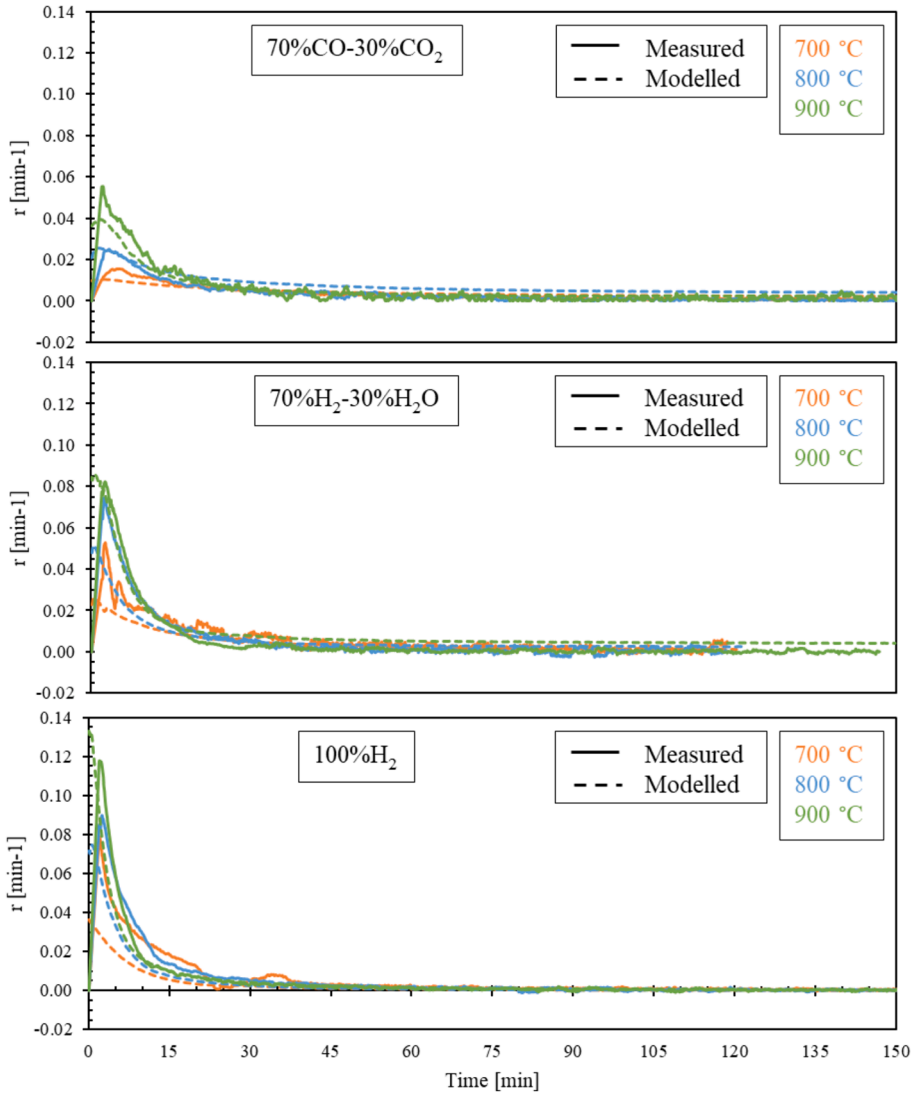

Fig. 8. The measured and modelled rate of mass loss for Nchwaning ore for each reducing atmosphere at the selected temperatures.

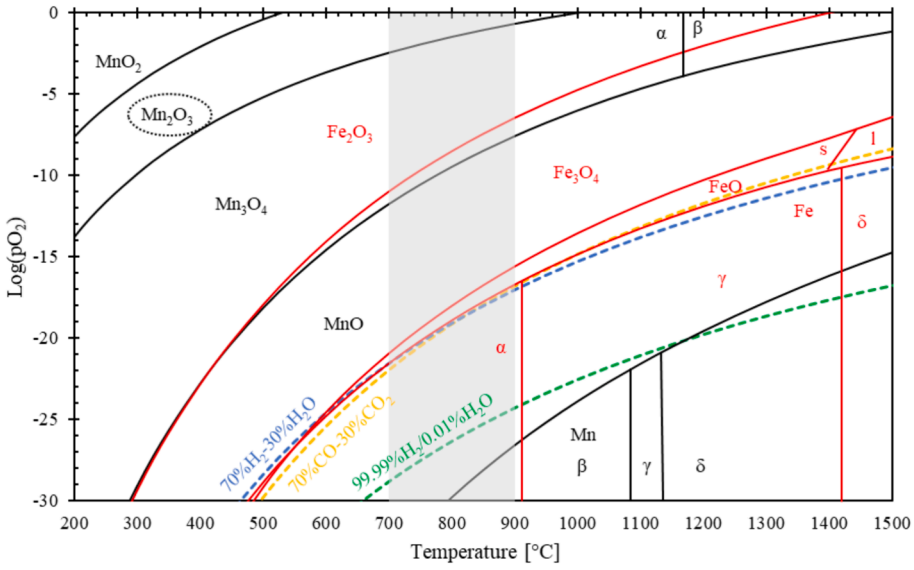

Fig. 9. The Mn-O and Fe-O stability diagrams with pO_2 as a function of temperature and the reducing atmospheres with pO_2 as a function of temperature. Databases used: FToxide, FTmisc, FactPS.

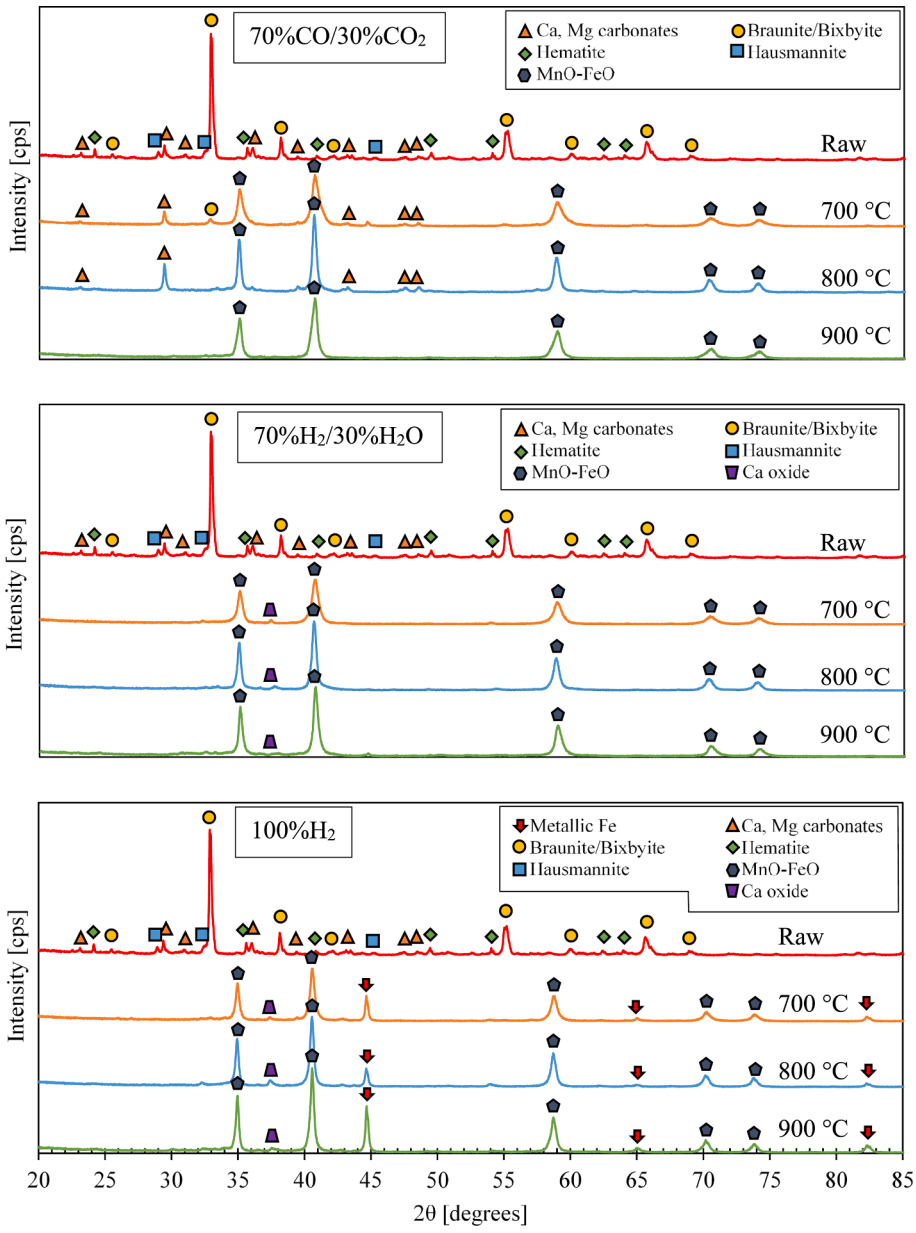

Fig. 10. The phase transformation for each reducing atmosphere at the selected temperatures.

are detected at 700, 800, and 900 °C. The calcite decomposition resulted in the formation of Ca-oxide (CaO) and is detected at 700, 800, and 900 °C, with the same peak intensities. The reason for no peaks in Mg-oxide (MgO), is that it is insignificant small compared to CaO. From the raw Mn ore chemical analysis (Table 2), $\mu(CaO)_{(i)} = 7.6$ mass% and $\mu(MgO)_{(i)} < 1$ mass%. This indicated that there is also significantly more $CaCO_3$ than $MgCO_3$ in the raw ore. All the higher Mn- and Fe-oxides are reduced to MnO and FeO at all three temperatures.

For samples pre-reduced in the H_2 atmosphere, again no carbonates are detected at 700, 800, and 900 °C, due to complete carbonate decomposition. Similar to the H_2/H_2O atmosphere, CaO was detected at all three temperatures. The braunite/bixbyite as well as the hematite and hausmannite phases all reduced to MnO and FeO. Metallic Fe is also detected at all three temperatures. This suggests that a pure H_2 atmosphere has enough reduction potential to reduce higher Fe-oxides to metallic Fe (Davies, Paktunc, *et al.*, 2022; Davies, Tangstad, *et al.*, 2022; Pineau et al., 2006, 2007; Piotrowski et al., 2005). The intensities of both the MnO-FeO and metallic Fe peaks increase as the temperature increases.

The absence of the intermediary hausmannite from the presented refractrographs is a result of the direct reduction of the present Mn-oxides to MnO due to the increased reduction rate at higher temperatures, as well as the rapid reduction due to the inclusion of H_2 (Zaki et al., 1997). Complete Mn-oxide reduction occurred in all cases, according to the chemical analysis, where $\mu(MnO_2)_{(i)} < 0.05$ mass% after pre-reduction. As previously mentioned, it is assumed from the chemical analysis methods, that all the Mn absent from MnO_2 is in MnO. Thus, the O/Mn is equal to 1.00 after pre-reduction, which is confirmed by Figure 1 in the Supplementary document.

3.5. Decrepitation analysis

Decrepitation is an undesired phenomenon, as the presence of fines in a furnace limits gas permeability and can prevent pre-reduction of the Mn ores in the upper part of the furnace (Biørnstad, 2020). However, a small particle size will result in an increased reaction rate due to an increase in the particle surface area, and subsequently, a decreased time for total conversion (Ngoy et al., 2020). Thus, for optimal furnace

operation, an ideal particle size is required with minimal decrepitation occurring.

In this case, the initial particle size ranged from 9.5 – 16 mm. Decrepitation is a result of internal stress due to a combination of various factors. These factors are uneven particle heating profiles, phase transformation that forms anisotropy, elimination of structural water, and carbonate decomposition (Biørnstad, 2020; Faria et al., 2013). After sieving the raw and pre-reduced ore with the selected sieves (9.5, 6.7, 4.75, 3.15, 1.6, and 0.5 mm), the over-size is documented to present the data in cumulative plots. The fraction for every reducing atmosphere at each temperature is illustrated in Fig. 11.

From Fig. 11 it is seen that the average decrepitation is 35 – 37 % for the CO/CO_2 atmosphere, with 5 % more fines formation at 800 °C. There is a bigger range of decrepitation over the selected temperatures for the H_2/H_2O atmosphere. At 700 °C the average decrepitation is 53 % whereas it is 29 % at 900 °C. The average decrepitation is 33 – 39 % for the H_2 atmosphere, relatively similar to that in the CO-CO_2 atmosphere. Davies et al. (2023) reported that the decrepitation for UMK Mn ore is 45 – 55 % for the same atmospheres and temperatures. This is likely a result of the higher carbonate content (17.0 mass%) in their ore that resulted in higher decrepitation.

Decrepitation is relatively constant over the temperature range for the H_2 and CO/CO_2 atmospheres. However, there is a strong negative correlation between decrepitation in the H_2/H_2O atmosphere and temperature. The observed phenomenon is attributed to the presence of water vapour in a reducing atmosphere. At 700 °C, water vapour likely condenses into the liquid phase more frequently than at 900 °C. The liquid phase molecules formed during the reaction undergo evaporation, with some immediately evaporating and others entering pores before evaporating. This evaporation-induced expansion creates internal pressure, leading to the cracking of samples. The extent of this effect is more significant at 700 °C compared to 900 °C, resulting in more pronounced decrepitation at the lower temperature.

3.6. Porosity analysis

Porosity measures the amount of volume in a bulk sample that is not the actual sample material. This is obtained by the ratio of the absolute

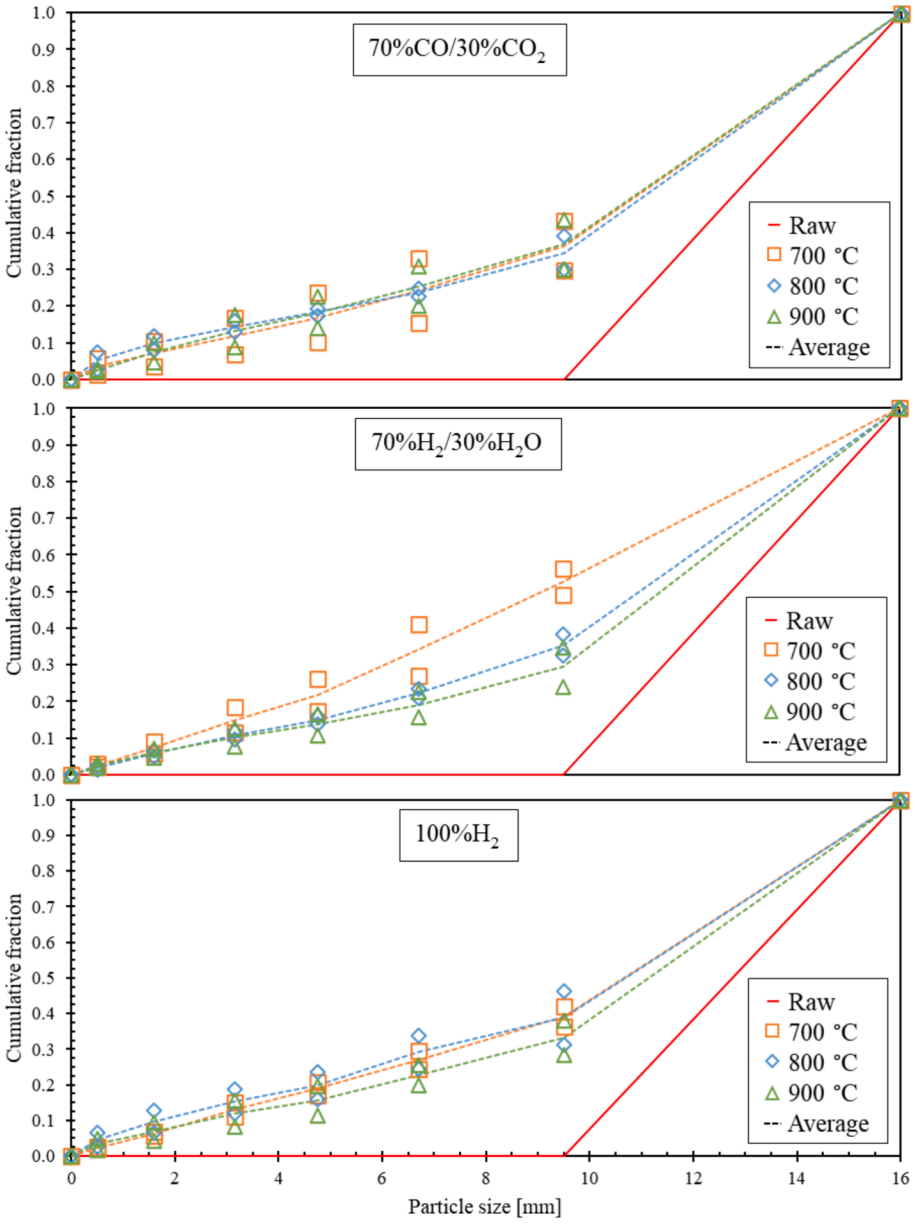

Fig. 11. Decrepitation for each reducing atmosphere at the selected temperature.

to the apparent density of a particle. A higher porosity indicates a larger surface area of a sample for solid–gas reactions to occur, which in turn promotes the reduction rate of Fe- and Mn-oxides and increases the reactivity of the ore (Pochart et al., 2007). However, the drawback of high porosity is the low thermal strength (Visser et al., 2013). The higher porosity signifies an increased ability to absorb moisture and when the ore is then rapidly heated, evaporated internal moisture asserts high pressure on the internal structure of the ore particles (Faria et al., 2013). This causes the particles to fracture easily when subjected to extreme heat. The average porosity of three particles in each sample is depicted in Fig. 12.

In Fig. 12, the formation of pores during the pre-reduction can be observed. The porosity of the raw ore is 0 %, due to no heat treatment (Biørnstad, 2020). For the ore heated in Ar for 1 h, the average porosity increased to 4 – 8 % over the temperature range, whereas for the pre-reduced ore, it increased to 20 – 38 %. The grouping at 900 °C is much closer due to a smaller distribution of the apparent density at 900 °C and at 700 °C, more pores formed in the presence of H_2. This could be due to the strong reduction drive force of H_2, as the porosity is also the most by a fraction in the presence of H_2 at 900 °C. However, the random selection of particles for porosity measurement is not representative enough of the whole case.

The last two properties, namely decrepitation and porosity, do not have a direct link with temperature changes, but rather with the amount of time samples are subjected to a heated environment. Decrepitation during the heating phase and porosity are proportional to the time spent in the heated environment. For instance, the longer the samples experience high temperatures, the longer there is time for carbonate to decompose and oxides to reduce. This, in turn, results in a weakened and fragile material structure. Hence, porosity will increase to 4 – 38 % over the period, as well as decrepitation during the heating phase to 16 – 34 % over the period.

4. Conclusions

In conclusion, the experimental investigation has provided significant insights into the temperature- and atmosphere-dependent behaviours of carbonate decomposition and oxide reduction in Nchwaning ore.

The study demonstrates a direct relationship between temperature and carbonate decomposition, with subsequent reduction of higher Mn- and Fe-oxides observed as temperatures rise. The introduction of different gaseous reducing atmospheres significantly affects carbonate decomposition and mass loss, with H_2-containing atmospheres facilitating near-complete carbonate decomposition and increased mass loss rates, especially through the reduction of higher Fe-oxides to metallic Fe during pure H_2 pre-reduction.

Moreover, decreasing pO_2 promotes the reduction of higher Mn- and Fe-oxides, contributing substantially to overall mass loss. The analysis also highlights the influence of temperature on the rate and equilibrium time of mass loss, as well as the O/Mn, with increasing temperature leading to faster reduction rates and quicker equilibrium times. Additionally, the inclusion of H_2 in the atmosphere accelerates the decline of O/Mn, increases mass loss rates, and elevates pre-exponential constants, while a decrease in pO_2 further enhances these trends. Furthermore, properties such as decrepitation and porosity are more affected by the duration of exposure to high temperatures rather than the temperature itself, except for decrepitation during H_2/H_2O pre-reduction, which exhibits a strong negative correlation with temperature. Overall, these findings underscore the complex interplay between temperature, reducing atmospheres, and ore properties, providing valuable insights for optimizing ore processing and refining strategies in industrial applications.

It is recommended to develop a high-temperature batch furnace for pre-reducing Mn ore with H_2 to produce a MnO-rich material. The process would involve using raw Mn ore and H_2 gas as feed materials, with water vapour generated as a by-product. The resulting product would consist of MnO and Fe-rich processed ore, possibly containing other oxides such as FeO and CaO from metal carbonates present in the raw ore. This processed ore could then be utilised as feed material for HC-FeMn production. To ensure sustainability, the H_2 should be produced using renewable energy sources such as solar, wind, or hydroelectric power, for instance, through H_2 electrolysis cells. Additionally, the water vapour by-product can be purified and utilized as a heat source, while the condensed water can be recycled back to the H_2 electrolysis cell, contributing to a closed-loop system.

CRediT authorship contribution statement

M.S. ERNST: Writing – review & editing, Writing – original draft, Visualization, Validation, Investigation, Formal analysis, Data curation. **M. TANGSTAD:** Writing – review & editing, Writing – original draft, Validation, Supervision, Resources, Project administration, Methodology, Funding acquisition, Formal analysis, Data curation,

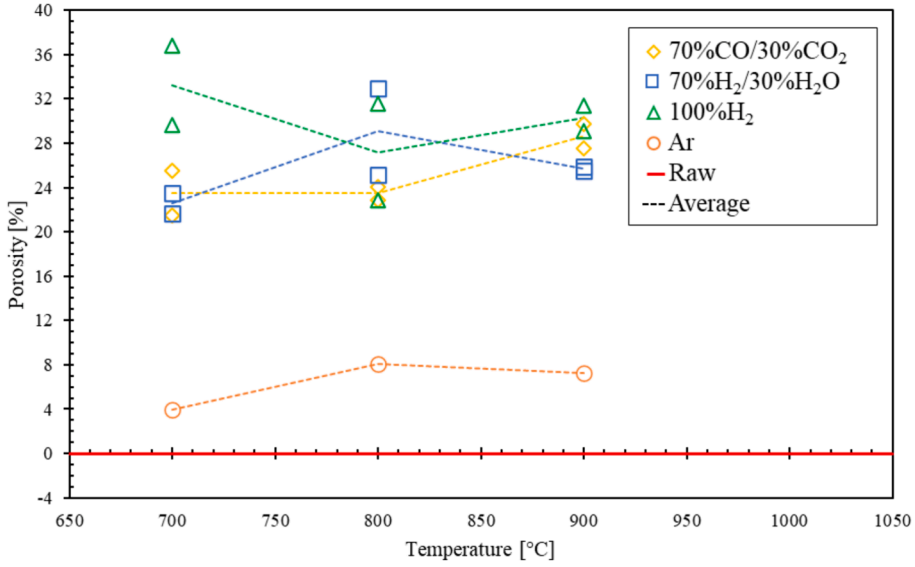

Fig. 12. The porosity of the raw, heated, and pre-reduced Nchwaning ore for each reducing atmosphere at each selected temperature.

Conceptualization. **S.P. DU PREEZ:** Writing – review & editing, Writing – original draft, Validation, Supervision, Project administration, Methodology, Investigation, Funding acquisition, Formal analysis, Conceptualization.

Declaration of competing interest

The authors declare that they have no known competing financial interests or personal relationships that could have appeared to influence the work reported in this paper.

Data availability

The data that has been used is confidential.

Acknowledgements

This study was supported by the Research Council of Norway (RCN) as the Thanos project (INPART Project 309475) and by HySA Infrastructure Centre of Competence, Department of Science and Innovation (DSI) South Africa, through the KP5 program, and are gratefully acknowledged.

Appendix

The O/Mn of the pre-reduced samples under different reducing atmospheres over the 700 – 900 °C temperature range is depicted in Figure 1.

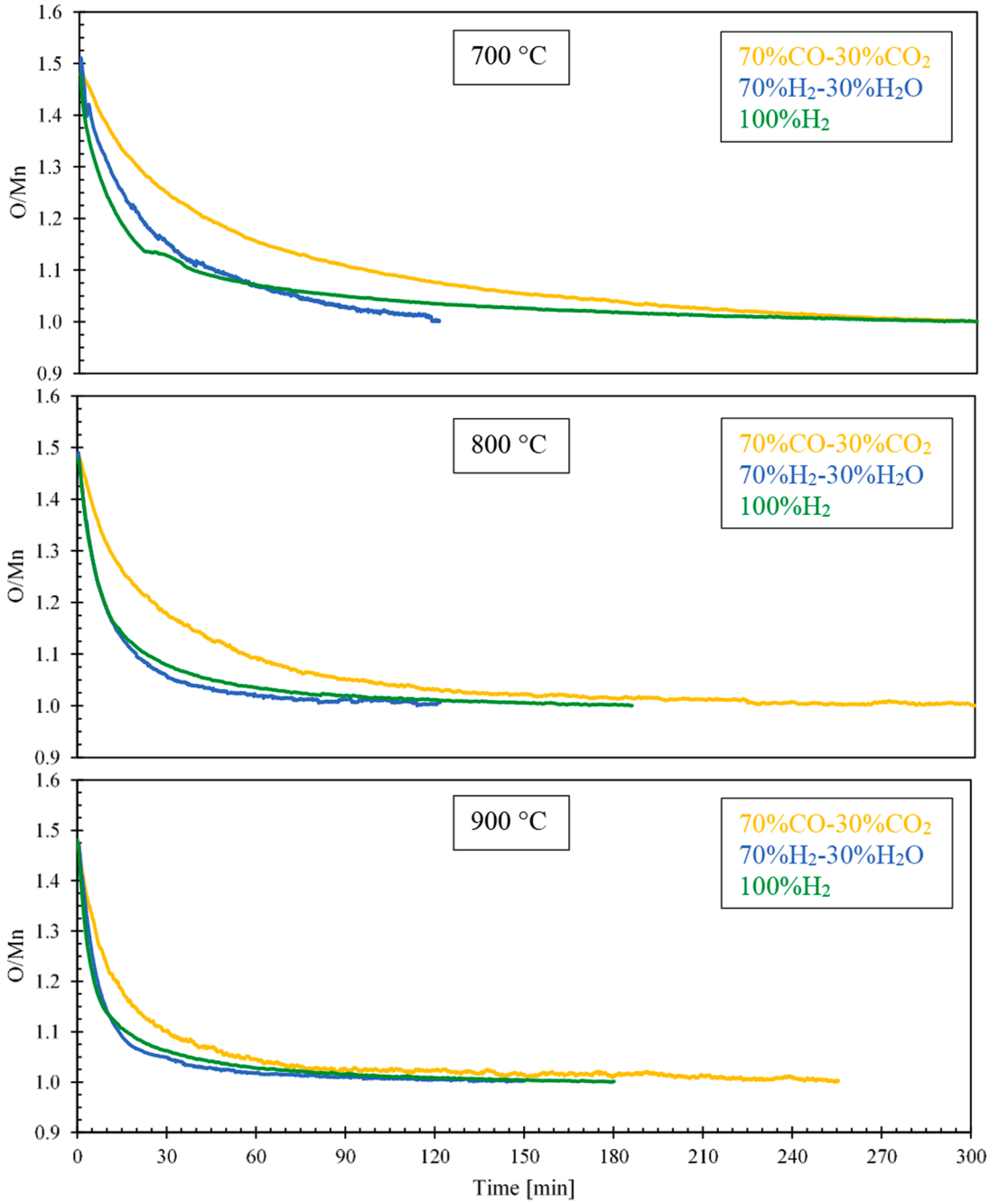

Fig. 1. The O/Mn as a function of time for the reducing atmospheres at the selected temperatures.

References

Acharya, C., Kar, R.N., Sukla, L.B., Misra, V.N., 2004. Fungal leaching of manganese ore. Trans. Indian Inst. Met. 57 (5), 501–508.

Bale, C.W., Bélisle, E., Chartrand, P., Decterov, S.A., Eriksson, G., Gheribi, A.E., Hack, K., Jung, I.H., Kang, Y.B., Melançon, J., Pelton, A.D., Petersen, S., Robelin, C., Sangster, J., Spencer, P., Van Ende, M.-A., 2016. FactSage Thermodynamical Software and Databased - 2010–2016. Calphad 54, 35–53.

K. Bergman B. Kjellberg DC Arc Furnace Technology Applied to Smelting Applications 2001 Quebec City 80 89.

Biørnstad, O., 2020. In: Decrepitation of Comilog, Assmang and UMK Manganese Ores during Prereduction. Norwegian University of Science and Technology, Trondheim, pp. 1–85.

Chen, G., Ling, Y., Li, Q., Zheng, H., Omran, M., He, F., 2020. Investigation on microwave carbothermal reduction behavior of low-grade pyrolusite. J. Mater. Res. Technol. 9 (4), 7862–7869.

Cheng, H., Reiser, D.B., Dean, S., 1999. On the mechanism and energetics of Boudouard reaction at FeO(1 0 0) surface: $2CO \rightarrow C+CO_2$. Catal. Today 50, 579–588.

Cheraghi, A., Yoozbashizadeh, H., Safarian, J., 2020. Gaseous reduction of manganese ores: A review and theoretical insight. Miner. Process. Extr. Metall. Rev. 41 (3), 198–215.

Corathers, L.A., 2020. 2020 Mineral Commodity Summary: Manganese. Reston, Virginia https://pubs.usgs.gov/periodicals/mcs2020/mcs2020-manganese.pdf.

Corathers, L.A., 2023. 2021 Minerals Yearbook: Manganese. Reston, Virginia https://d9-wret.s3.us-west-2.amazonaws.com/assets/palladium/production/s3fs-public/media/files/myb1-2021-manga-ert.xlsx.

L.A. Corathers 2014 Minerals Yearbook: Manganese Reston Virginia. 2017 https://d9-wret.s3.us-west-2.amazonaws.com/assets/palladium/production/mineral-pubs/manganese/myb1-2014-manga.pdf.

Criado, J.M., Gonzalez, F., Gonzalez, M., 1982. Influence of the CO_2 pressure on the kinetics of thermal decomposition of manganese carbonate. J. Therm. Anal. 24, 59–65.

Davies, J., Tangstad, M., Ringdalen, E., Beukes, J.P., Bessarabov, D., Du Preez, S.P., 2022a. The Effect of Pre-Oxidation on the Reducibility of Chromite Using Hydrogen: A Preliminary Study. Minerals. 12 (7), 911.

Davies, J., Paktunc, D., Ramos-Hernandez, J.J., Tangstad, M., Ringdalen, E., Du Preez, S. P., 2022b. The Use of Hydrogen as a Potential Reductant in the Chromite Smelting Industry. Minerals. 12 (5), 534.

Davies, J., Tangstad, M., Schanche, T.L., Du Preez, S.P., 2023. Pre-reduction of United Manganese of Kalahari Ore in CO/CO_2, H_2/H_2O, and H_2 Atmospheres. Metall. Mater. Trans. B 54 (2), 515–535.

Du Preez, S.P., Van Kaam, T.P.M., Ringdalen, E., Tangstad, M., Morita, K., Beukes, J.P., 2023. An Overview of Currently Applied Ferrochrome Production Processes and Their Waste Management Practices. Minerals. 13 (6), 809.

Eissa, M., Ghali, S., Ahmed, A., El-Faramawy, H., 2012. Optimum condition for smelting high carbon ferromanganese. Ironmak. Steelmak. 39 (6), 419–430.

Eric, R.H. 2014. Production of Ferroalloys. In: *Treatise on Process Metallurgy*. Elsevier. pp. 477–532.

G.L. Faria J.A.S. Tenório N. Jannotti da S. Araújo, F.G. Disintegration on heating of a Brazilian manganese lump ore Int. J. Miner. Process. 124 2013 132 137.

Kalenga, M., Xiaowei, P., Tangstad, M., 2013. Manganese alloys production: Impact of chemical compositions of raw materials on the energy and materials balance. In: In: *Proceedings of the 13th International Ferroalloys Congress (INFACONXIII)*. Almaty, pp. 647–654.

Larssen, T.A., Tangstad, M., 2022. Effect of moisture, hydrogen, and water–gas shift reaction on the prereduction behaviour of Comilog and Nchwaning manganese ores. Metall. Mater. Trans. B 53 (4), 2104–2116.

Larssen, T.A., Senk, D., Tangstad, M., 2021. Reduction of Manganese Ores in $CO\text{-}CO_2$ Atmospheres. Metall. Mater. Trans. B 52 (1), 363–381.

Ngoy, D., Sukhomlinov, D., Tangstad, M., 2020. Pre-reduction behaviour of manganese ores in H_2 and CO containing gases. ISIJ Int. 60 (11), 2325–2331.

Ngoy, D.M., Tangstad, M., Kalenga, M., 2018. Reduction rate of MnO from two different manganese ores producing ferromanganese. In: In: *Proceedings of the 15th International Ferroalloys Congress (INFACONXV)*. Cape Town, pp. 207–218.

Olsen, S.E., Tangstad, M., Lindstad, T., 2007. Production of manganese ferroalloys. Tapir Academic Press, Trondheim.

Pineau, A., Kanari, N., Gaballah, I., 2006. Kinetics of reduction of iron oxides by H_2. Part i. *Thermochimica Acta*. 447 (1), 89–100.

Pineau, A., Kanari, N., Gaballah, I., 2007. Kinetics of reduction of iron oxides by H_2. Part II. *Thermochimica Acta*. 456 (2), 75–88.

Piotrowski, K., Mondal, K., Lorethova, H., Stonawski, L., Szymanski, T., Wiltowski, T., 2005. Effect of gas composition on the kinetics of iron oxide reduction in a hydrogen production process. Int. J. Hydrogen Energy 30 (15), 1543–1554.

G. Pochart L. Joncourt N. Touchard C. Perdon Metallurgical Benefit of Reactive High Grade Ore in Manganese Alloys Manufacturing 2007 New Delhi 217 230.

Roine, A. 2017. HSC Chemistry for Windows, v. 10 (Pori, Finland: Outotec Research, 2017). https://www.hsc-chemistry.com/news&tiedoteid=31.

Schanche, T.L., Tangstad, M., 2021. Prereduction of Nchwaning ore in $CO/CO_2/H_2$ gas mixtures. Minerals. 11 (10), 1097.

Tangstad, M., 2013. Manganese ferroalloys technology. In: Gasik, M. (Ed.), Handbook of Ferroalloys Theory and Technology. Butterworth-Heinemann, Oxford, pp. 221–266.

Tangstad, M., Schanche, T., Du Preez, S.P., 2023. Use of H_2 in Mn-Ferroalloy Production. Minerals, Metals and Materials Series, pp. 35–53.

Valverde, J.M., Perejon, A., Medina, S., Perez-Maqueda, L.A., 2015. Thermal decomposition of dolomite under CO2: insights from TGA and in situ XRD analysis. PCCP 17 (44), 30162–30176.

Visser, M., Smith, H., Ringdalen, E., Tangstad, M., 2013. Properties of Nchwaning and Gloria ores in the production of Mn Ferro-alloys. In: In: *Proceedings of the 13th International Ferroalloys Congress (INFACONXIII)*. Almaty, pp. 553–566.

Vogl, V., Olsson, O., Nykvist, B., 2021. Phasing out the blast furnace to meet global climate targets. Joule. 5 (10), 2646–2662.

Wang, Y., Lin, S., Suzuki, Y., 2007. Study of limestone calcination with CO_2 capture: decomposition behaviour in a CO_2 atmosphere. Energy Fuel 21, 3317–3321.

Zaki, M.I., Hasan, M.A., Pasuplety, L., Kumari, K., 1997. Thermochemistry of manganese oxides in reactive gas atmospheres: Probing redox compositions in the decomposition course MnO_2 to MnO. Thermochim Acta 303, 171–181.